## PROCEEDINGS OF SPIE

SPIEDigitalLibrary.org/conference-proceedings-of-spie

# Temporal evolution of sky polarization during solar eclipse totality

Joseph A. Shaw, Laura M. Eshelman, Martin Jan Tauc, Glenn E. Shaw

Joseph A. Shaw, Laura M. Eshelman, Martin Jan Tauc, Glenn E. Shaw, "Temporal evolution of sky polarization during solar eclipse totality," Proc. SPIE 11132, Polarization Science and Remote Sensing IX, 111320C (6 September 2019); doi: 10.1117/12.2531269



Event: SPIE Optical Engineering + Applications, 2019, San Diego, California, United States

### Temporal evolution of sky polarization during solar eclipse totality

Joseph A. Shaw\*a, Laura M. Eshelmana, Martin Jan Tauca, Glenn E. Shawc

<sup>a</sup>Electrical & Computer Engineering Dept., Montana State University, Bozeman, MT USA 59717; <sup>b</sup>Polaris Sensor Technologies, Inc., Huntsville, AL USA 35801; <sup>c</sup>Geophysical Institute, University of Alaska, Fairbanks, AK USA 99775

#### **ABSTRACT**

The sky polarization pattern during solar eclipse totality shifts from the usual daytime clear-sky pattern, with maximum polarization in an arc located 90° from the Sun, to one with maximum polarization slightly above the horizon in a ring nominally concentric about the zenith. A sequence of 9 visible-wavelength all-sky images are shown throughout totality for the 21 August 2017 solar eclipse from a site near Rexburg, ID USA (43.8294°N, 111.8849°W). A neutral region appeared in the southwest quadrant of the all-sky images, directly opposite the eclipsed Sun, and evolved in size and radial position throughout the 2 min 17 s of totality.

**Keywords:** Polarization, scattering, atmospheric optics, solar eclipse, remote sensing

#### 1. INTRODUCTION

During solar eclipse totality, the sky polarization pattern changes dramatically because the light source abruptly switches from direct sunlight to sunlight that has been multiply scattered into the umbra from outside the umbra. This leads to the polarization pattern shifting from the usual clear-sky pattern, with maximum polarization in an arc located 90° from the Sun, to a pattern with maximum polarization slightly above the horizon in a ring nominally concentric about the zenith. This was first shown by Glenn Shaw at the 1973 eclipse in Kenya<sup>1,2</sup> and the small asymmetry in his measurements were suggested to be a possible result of asymmetric surface albedo below the umbra (with a dark lake on one side and bright desert on the other side). Können developed a simple model that extended the prediction of symmetry about the zenith and hypothesized that the asymmetry in Shaw's African measurements was a result of the changing conditions during the scan time for Shaw's scanning polarimeter.<sup>3</sup> More recently, all-sky polarization imaging has been used to reveal evidence of a significantly asymmetric pattern of sky polarization during solar eclipse totality.<sup>4,5,6</sup> For the 21 August 2017 eclipse, our goal was to use our own experience with all-sky polarization imaging and related remote sensing measurements to characterize aerosols, clouds, and surface reflectance, and thereby obtain the most complete data set based on all-sky images of sky polarization during solar eclipse totality.<sup>7,8</sup>

The eclipse polarization measurements were the latest step in a long history of polarization remote sensing research conducted by our research group, first at the National Oceanic and Atmospheric Administration (NOAA) with numerical and experimental studies of thermal infrared polarization from water. 9-13 The most recent 18 years of this history have taken place at Montana State University, where we have pursued all-sky polarization imaging to quantify the dependence of VIS/NIR sky polarization on aerosols, clouds, and surface reflectance. Our primary instrument has been a multiwavelength VIS/NIR all-sky polarization imager based on liquid crystal variable retarders <sup>14</sup> (LCVRs) to achieve a rapid sequence of all-sky images at different retardance states so we can retrieve a full Stokes vector at each pixel while avoiding the time smearing that plagues slower division-of-time polarimeters.<sup>15</sup> Deploying this imager continuously outdoors<sup>16</sup> allowed us to obtain radiometrically and polarimetrically accurate images even with variable clouds so we could quantify how clouds alter the clear-sky degree of linear polarization (DoLP) and under certain conditions even the angle of polarization.<sup>17</sup> Comparisons were made with simple radiative transfer models<sup>18,19</sup> and more complex radiative transfer models.<sup>20</sup> The LCVR all-sky polarization imager was deployed at the Mauna Loa Observatory in Hawaii to quantify the role of surface reflectance on the clear-sky DoLP<sup>21</sup> and this was incorporated into a model that was used to explain the huge spectral variation of DoLP in the VIS/NIR spectral range<sup>22</sup> and later the VIS-SWIR spectral range.<sup>23</sup> Recently we have used all-sky polarization imaging for remote sensing of cloud thermodynamic phase.<sup>24-26</sup> This paper now builds on a previous proceedings paper8 to summarize the temporal evolution of the 2017 eclipse sky polarization.

\*joseph.shaw@montana.edu; phone 1 406 994-7261; fax 1 406 994-5958; http://www.montana.edu/jshaw/

Polarization Science and Remote Sensing IX, edited by Julia M. Craven, Joseph A. Shaw, Frans Snik, Proc. of SPIE Vol. 11132, 111320C ⋅ © 2019 SPIE ⋅ CCC code: 0277-786X/19/\$21 ⋅ doi: 10.1117/12.2531269

#### 2. MEASUREMENT METHODS

#### 2.1 All-sky polarization imagers

For the 2017 solar eclipse we developed two all-sky polarization imagers, each based on three digital single-lens-reflex (DSLR) cameras with fisheye lenses,  $^7$  to take images faster than is possible with the LCVR system during the low-light conditions of totality. One of these new 3-camera systems was based on Nikon D700 DSLR cameras with Sigma 14-mm f/2.8 fisheye lenses, while the other new 3-camera system was based on Sony  $\alpha$ 7s cameras. We originally built the Nikon system using existing cameras and then later built the Sony system for redundancy when we found that we could get a commercial adapter to couple the Nikon-mount Sigma fisheye lenses to the Sony E-mount bodies. Having two all-sky polarization imaging systems based on different DSLR bodies ended up also providing valuable confirmation of the spatially variable patterns we measured, as both systems (which were oriented side by side, but with one rotated 180° in azimuth from the other one) measured effectively identical sky polarization patterns. The LCVR-based all-sky polarization imager 15,16 also was used, but only was able to capture one well-exposed totality image (but it also agreed with the results measured by the 3-camera systems at the same time).

We deployed our instruments at the BYU-Idaho astronomical observatory located at 43.8294°N, 111.8849°W, approximately 8.8 km from the center line of totality and 8 km west and slightly north of the BYU-Idaho campus in Rexburg, Idaho. This was an excellent site, with low ambient light pollution and excellent horizon-to-horizon views of the sky. Figure 1 shows three degree of linear polarization (DoLP) all-sky images on the top row and three angle of polarization (AoP) all-sky images on the bottom row, comprising three DoLP-AoP image pairs at sunrise (left), midday but post-totality (center) and near sunset (right). In each image, the outer edge of the circle is the horizon and the center is the zenith. These daytime images taken before and after the eclipse were measured with the LCVR imager's 450-nm channel. The AoP is shown relative to the solar principal plane containing the Sun, the zenith, and the observer. The allsky images are oriented with north to the top and west to the right. This requires care to avoid confusing east and west, but it matches what would be seen by an observer lying on the ground, looking up into the sky with his or her head pointing north. The DoLP images include a sun-occulter disk mounted on a metal band stretching across the lower portion of the image (moving to block the Sun as its position shifts from southeast in the morning to southwest in the evening). The band of maximum polarization situated 90° from the Sun has a DoLP value near 60%, higher in the morning than in the evening (note also that the DoLP is effectively zero at and very near the Sun). The lower DoLP at the end of the day was a result of higher aerosol optical depth that occurred as wildfire smoke concentration increased after a welcome break in haziness during morning and midday on the eclipse day. The AoP images also show the morning-to-evening evolution of the otherwise fixed pattern, with colored patterns coming together to indicate the location of the Babinet neutral point just above the Sun and a numerical discontinuity that has the appearance of another neutral point at the zenith (i.e., the center of the images).

One of the supporting instruments we deployed at this experiment was a new fisheye-lens-based all-sky infrared cloud imager (ICI) system based on a long history of thermal infrared imagers developed to detect and characterize clouds from the ground.<sup>27-34</sup> The ICI system was operated throughout eclipse day, detecting any clouds in the sky continuously, 24 hours per day. On the day of the eclipse (21 Aug. 2017), those images showed scattered clouds near the southeast horizon in the early morning hours before and near dawn but confirmed a completely cloud-free sky for the duration of the late-morning eclipse. Other supporting instruments included an AERONET<sup>35</sup> solar radiometer at the nearby BYU-Idaho campus and ground-level weather stations at BYU-Idaho and at the BYU-Idaho astronomical observatory where we were deployed (~8 km west-northwest of campus). Some of the data from these supporting instruments were shown in our earlier proceedings paper.<sup>8</sup>

#### 3. TOTALITY ALL-SKY POLARIZATION IMAGES

Even throughout the latest stages of partial eclipse, the rapidly darkening sky maintained its daytime-like polarization pattern, abruptly shifting to the nominally zenith-concentric pattern at second contact, which marked the start of totality (17:33:05 UTC = 11:33 am Mountain Daylight Time). Figure 2 is a multi-frame image showing all-sky DoLP images from the start of totality (upper left, 17:33:13) to the last second of totality (lower right, 17:35:23). Below each image is the UTC time when that image was recorded by the 3-camera Nikon all-sky polarization imaging system. Obstructions low on the horizon include two power poles and a small agricultural building at the upper left (NE of the imager), the observatory dome at the lower right (SW of the imager), and an excited student's head and hands (holding a camera) at the right side (W side) of the 17:34:24 and 17:34:36 images.

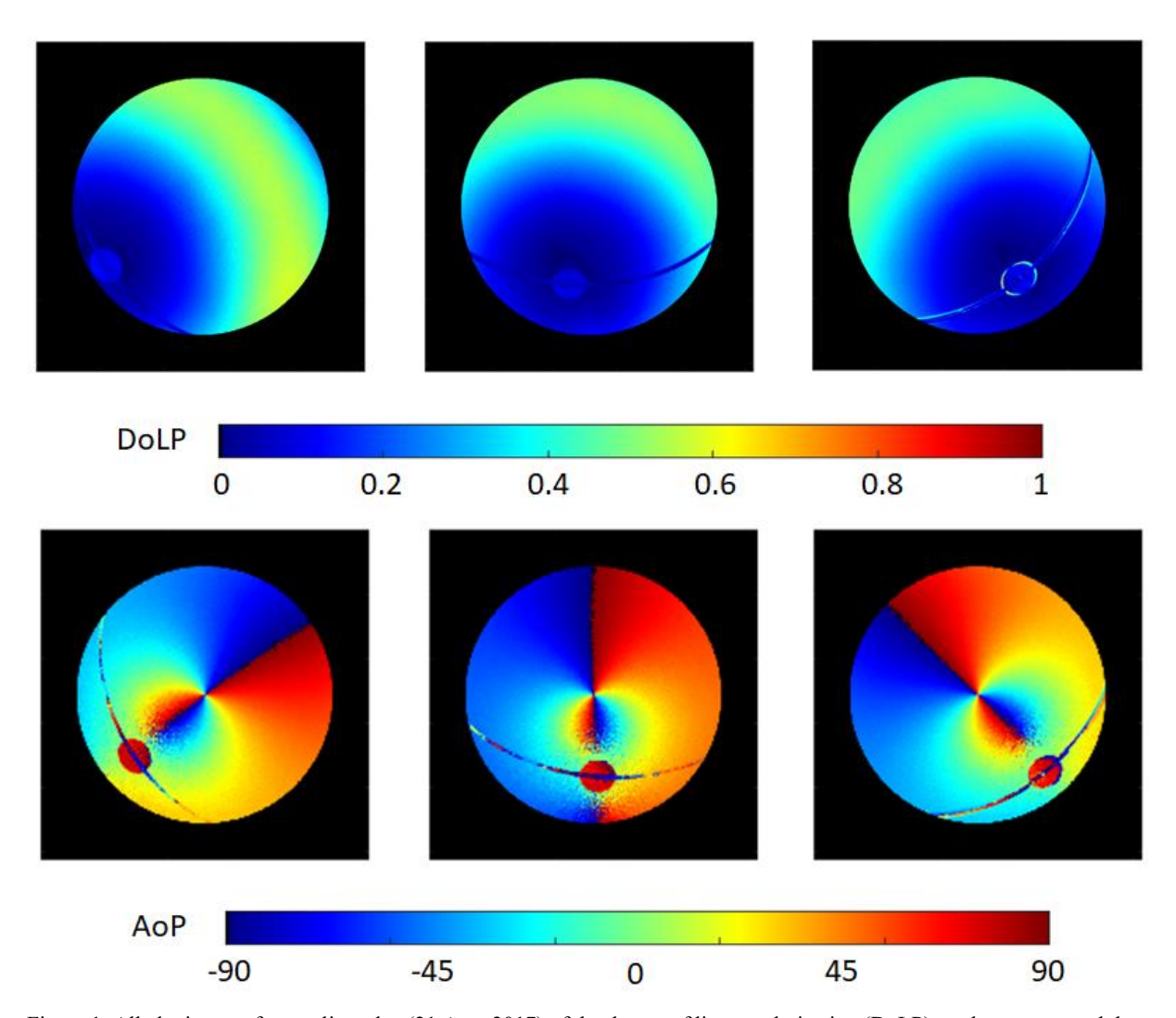


Figure 1. All-sky images from eclipse day (21 Aug. 2017) of the degree of linear polarization (DoLP) on the top row and the angle of polarization (AoP) on the bottom row. DoLP and AoP image pairs are shown for sunrise (left), midday (middle), and near sunset (right). The images are from the blue channel (~450 nm) of the LCVR all-sky polarization imager and the AoP is shown referenced to the solar principal plane. <sup>26</sup>

The polarization pattern that was otherwise fairly symmetric about the zenith exhibited a large neutral region with zero or minimal polarization in the portion of the sky directly opposite the Sun (i.e., the NW part of the sky), in the direction from which the umbra approached our location. Throughout totality, this neutral region flattened toward the horizon and spread out in azimuth as the umbra progressed over our observing location. The neutral region was least apparent in the image recorded in the last second of totality and most apparent in the first image, which was recorded 8 seconds after the start of totality. In the band of highest totality polarization, located near the horizon (especially in the north, east, and south portions of the images), the peak DoLP reached approximately 50% for the blue channel (see our paper about camera characterization<sup>7</sup> for details of the spectral bands). Immediately following the final image shown in Figure 2, the sky polarization pattern returned abruptly to the usual daytime pattern, even though only a tiny fraction of the Sun was directly illuminating the sky around us at that time.

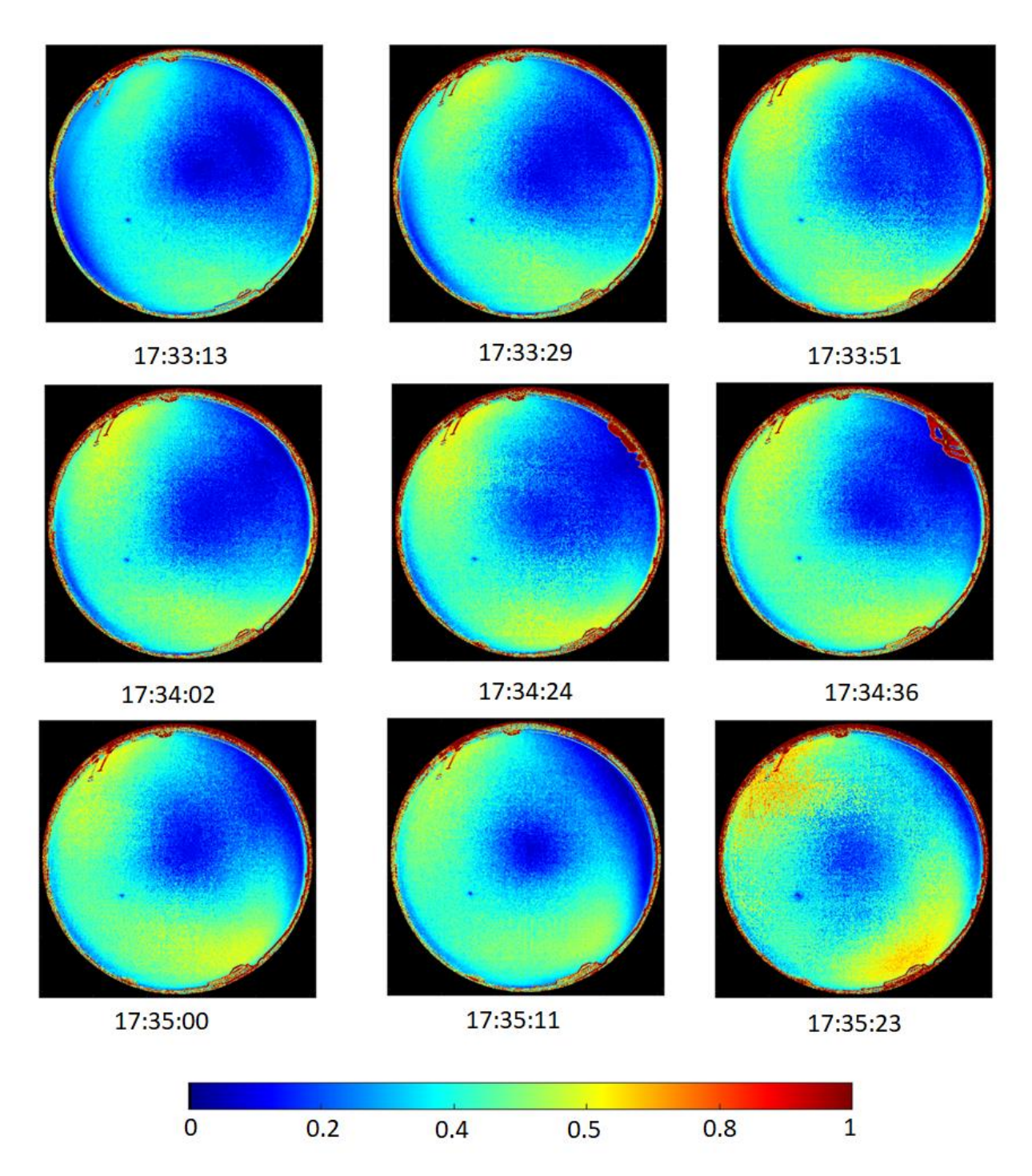


Figure 2. All-sky images of the degree of linear polarization (DoLP) at the indicated UTC times throughout totality on 21 Aug. 2017 in Rexburg, ID (43.8294°N, 111.8849°W). Obstructions low on the horizon include two power poles and a small agricultural building at the upper left (NE of the imager), the observatory dome at the lower right (SW of the imager), and an excited student's head and hands (holding a camera) at the right side (W side of the image) for the 17:34:24 and 17:34:36 images.

#### 4. CONCLUSIONS

Unlike the azimuthally symmetric pattern expected in early eclipse polarization papers, all-sky polarization imaging has revealed a very asymmetric pattern that evolves throughout totality. The images shown here were from the 21 August 2017 solar eclipse, observed near Rexburg, Idaho USA. This was a late-morning eclipse, with the umbra approaching from the northwest or top right region of the all-sky images shown here. The Sun was in the southeast or lower left region of the all-sky images shown here. A large neutral region with zero (or very nearly zero) polarization was observed in the northwest part of the sky, from where the umbra approached our observation site. This neutral region shifted toward the horizon and spread out in azimuth as totality progressed to third contact (end of totality). More details will be shown in a forthcoming journal paper.

#### **ACKNOWLEDGMENTS**

This material is based on research sponsored by the Air Force Research Laboratory, under agreement number FA955014-1-0140. The U.S. Government is authorized to reproduce and distribute reprints for Governmental purposes notwithstanding any copyright notation thereon. The views and conclusions contained herein are those of the authors and should not be interpreted as necessarily representing the official policies or endorsements, either expressed or implied, of the Air Force Research Laboratory or the U.S. Government.

#### REFERENCES

- [1] Shaw, G. E., "Sky brightness and polarization during the 1973 African eclipse," Appl. Opt. 14(2), 388-394 (1975).
- [2] Shaw, G. E., "Sky radiance during a total solar eclipse: a theoretical model," Appl. Opt. 17(2), 272-276 (1978).
- [3] Können, G. P., "Skylight polarization during a total eclipse: a quantitative model," J. Opt. Soc. Am. 4(3), 601-608 (1987).
- [4] Pomozi, I., Gal, J., Horvath, G., and Wehner, R., "Fine structure of the celestial polarization pattern and its temporal change during the total solar eclipse of 11 August 1999," Rem. Sens. Env. 76, 181-201 (2000).
- [5] Horvath, G., Pomozi, I., and Gal, J., "Neutral points of skylight polarization observed during the total eclipse on 11 August 1999," Appl. Opt. 42(3), 465-475 (2003).
- [6] Sipocz, B., Hegedus, R., Kriska, G., and Horvath, G., "Spatiotemporal change of sky polarization during the total solar eclipse on 29 March 2006 in Turkey: polarization patterns of the eclipsed sky observed by full-sky imaging polarimetry," Appl. Opt 47(34), H1-H10 (2008).
- [7] Hashimoto, T., Dahl, L. M., Laurie, S. A., and Shaw, J. A., "Camera characterization for all-sky polarization measurements during the 2017 solar eclipse", Proc. SPIE 10407, 1040706 (2017).
- [8] Eshelman, L. M. Tauc, M. J., Hashimoto, T., Hooser, P., Gillis, K., Weiss, W., Stanley, B., Shaw, G. E., and Shaw, J. A., "All-sky polarization measurements of the total solar eclipse on 21 August 2017," Proc. SPIE 10655, 106550L (2018).
- [9] Shaw, J. A., "Degree of linear polarization in spectral radiances from water-viewing infrared radiometers," Appl. Opt. 38(15), 3157-3165 (1999).
- [10] Iannarilli, F. J. Jr., Shaw, J. A., Jones, S. H., and Scott, H. E., "Snapshot LWIR hyperspectral polarimetric imager for ocean surface sensing," Proc. SPIE 4133, 270-283 (2000).
- [11] Shaw, J. A., "Polarimetric measurements of long-wave infrared spectral radiance from water," Appl. Opt. 40)33), 5985-5990 (2001).
- [12] Shaw, J. A., "Infrared polarization in the natural Earth environment," Proc. SPIE 4819, 129-138 (2002).
- [13] Shaw, J. A., The effect of instrument polarization sensitivity on sea surface remote sensing with infrared spectroradiometers," J. Atmos. Oceanic Technol. 19(5), 820-827 (2002).
- [14] Pust, N. J. and Shaw, J. A., "Dual-field imaging polarimeter using liquid crystal variable retarders," Appl. Opt. 45(22), 5470-5478 (2006).
- [15] Tyo, J. S., Goldstein, D. L., Chenault, D. B., and Shaw, J. A., "Review of passive imaging polarimetry for remote sensing applications," Appl. Opt. 45(22), 5453-5469 (2006).
- [16] Shaw, J. A., Pust, N. J., Staal, B., Johnson, J., and Dahlberg, A. R., "Continuous outdoor operation of an all-sky polarization imager," Proc. SPIE 7672, 76720A (2010).

- [17] Pust, N. J. and Shaw, J. A., "Digital all-sky polarization imaging of partly cloudy skies," Appl. Opt. 47(34), H190-H198 (2008).
- [18] Pust, N. J. and Shaw, J. A., "Comparison of skylight polarization measurements and MODTRAN-P calculations," J. Appl. Rem. Sens. 5(1), 053529 (2011).
- [19] Pust, N. J. and Shaw, J. A., "How good is a single-scattering model of visible-NIR atmospheric skylight polarization?," Proc. SPIE 7461, 74610B (2009).
- [20] Pust, N. J., Dahlberg, A. R., Thomas, M. J., and Shaw, J. A., "Comparison of full-sky polarization and radiance observations to radiative transfer simulations which employ AERONET products," Opt. Express 19(19), 18602-18613 (2011).
- [21] Dahlberg, A., Pust, N. J., and Shaw, J. A., "Effects of surface reflectance on skylight polarization measurements at the Mauna Loa Observatory," Opt. Express 19, 16008-16021 (2011).
- [22] Pust, N. J. and Shaw, J. A., "Wavelength dependence of the degree of polarization in cloud-free skies: simulations of real environments," Opt. Express 20(14), 15559-15568 (2012).
- [23] Eshelman, L. M. and Shaw, J. A., "The VIS-SWIR spectrum of skylight polarization," Appl. Opt. 57(27), 7974-7986 (2018).
- [24] Tauc, M. J., Baumbauer, C. L., Moon, B., Abel, A. M., Riesland, D. W., Eshelman, L. M., Nakagawa, W., and Shaw, J. A., "Cloud thermodynamic phase detection with a 3-channel shortwave infrared polarimeter," Proc. SPIE 10655, 106500 (2018).
- [25] Eshelman, L. M., Tauc, M. J., and Shaw, J. A., "All-sky polarization imaging of cloud thermodynamic phase," Opt. Express 27(3), 3528-3541 (2019).
- [26] Eshelman, L. M. and Shaw, J. A., "Visualization of all-sky polarization images referenced in the instrument, scattering, and solar principal planes," Opt. Eng. 58(8), 082418 (2019).
- [27] Shaw, J. A., Nugent, P. W., Pust, N. J., Thurairajah, B., and Mizutani, K., "Radiometric cloud imaging with an uncooled microbolometer thermal infrared camera," Opt. Express 13(15), 5807-5817 (2005).
- [28] Thurairajah, B. and Shaw, J. A., "Cloud statistics measured with the infrared cloud imager (ICI)," IEEE Trans. Geosci. Rem. Sens. 43(9), 2000-2007 (2005).
- [29] Nugent, P. W., Shaw, J. A., and Piazzolla, S., "Infrared cloud imaging in support of Earth-space optical communication," Opt. Express 17(10), 7862-7872 (2009).
- [30] Shaw, J. A. and Nugent, P. W., "Physics principles in radiometric infrared imaging of clouds in the atmosphere," Eur. J. Phys. 34(6), S111 (2013).
- [31] Nugent, P. W., Shaw, J. A., and Pust, N. J., "Correcting for focal-plane-array temperature dependence in microbolometer infrared cameras lacking thermal stabilization," Opt. Eng. 52(6), 061304 (2013).
- [32] Nugent, P. W., Shaw, J. A., and Pust, N. J., "Radiometric calibration of infrared imagers using an internal shutter as an equivalent external blackbody," Opt. Eng. 53(12), 123106 (2014).
- [33] Nugent, P. W. and Shaw, J. A., "Calibration of uncooled LWIR microbolometer imagers to enable long-term field deployment," Proc. SPIE 9071, 90710V (2014).
- [34] Redman, B. J., Shaw, J. A., Nugent, P. W., Clark, R. T., and Piazzolla, S., "Reflective all-sky thermal infrared cloud imager," Opt. Express 26(9), 11276-11283 (2018).
- [35] Holben, B. N., Eck, T. F., Slutsker, I., Tanré, D., Buis, J. P., Setzer, A., Vermote, E., Reagan, J. A., Kaufman, Y. J., Nakajima, T. Lavenu, F., Jankowiak, I., Smirnov, A, "AERONET—A federated instrument network and data archive for aerosol characterization," Rem. Sens. Env. 66(1), 1-16 (1999).